INTERNATIONAL JOURNAL FOR NUMERICAL METHODS IN FLUIDS, VOL. 6, 83–100 (1986)

UNSTEADY COMPRESSIBLE FLOW IN LONG PIPELINES FOLLOWING A RUPTURE

RENÉ FLATT

Swiss Federal Institute of Technology of Lausanne, CH-1015 Lausanne, Switzerland

SUMMARY

The unsteady frictional flow of a compressible fluid generated in a long pipeline after an accidental rupture is of considerable interest to the offshore gas industry. It answers several important questions concerning safety and pollution, e.g. the flow rate at the broken pipe end.

Laboratory tests cannot simulate the rather complex phenomenon satisfactorily. The problem is highly non-linear and no general analytical solution is yet known.

In this study, based on computational fluid dynamics, the simplifying assumptions of isothermal and low Mach number flow often applied in the case of unsteady compressible flows in pipelines, have not been used.

Owing to the choking condition ($Ma = 1$) which prevails for some time at the broken end, and the cumulative effect of friction over the 145 km long pipeline, we obtain $(\partial p/\partial x)_t \to -\infty$. This analytically established singularity leads to numerical difficulties which seriously affect the accuracy. For short tubes (such as shock tubes) this negative feature is much less severe. Special procedures were necessary to keep the accuracy within the chosen limit of 1 per cent.

KEY WORDS Flow Gas Numerical One-dimensional Pipeline Unsteady

1. INTRODUCTION

The amount of natural gas in a 145 km long offshore pipeline is about 7000 tons. This quantity is about one third of the crude lost during the famous BRAVO blowout in 1977 in the EKOFISK field in the North Sea. To obtain a more intuitive idea of this quantity we may think of it as a heat source delivering (after combustion) a heat power of 100 MW for 40 days (960 hours).

Pollution and economic losses due to the spilling of fuel may therefore be equally high for a blowout in an offshore well as in a pipeline on the sea-bed. Various efforts have been made to control the former,[1,2] but not much attention has yet been given to the latter.

The mass-flow of gas escaping from a burst pipeline is several orders of magnitude larger than the mass-flow from a spilling well. The former case represents a much more severe hazard in several ways. It may for instance cause instability (due to a partial loss of buoyancy) of platforms or ships caught in the top of the resulting water-gas plume.

The question arises how much the mass-flow released by a ruptured pipeline may amount to and how quickly it will diminish with time. From the fluid mechanics point of view this is a complicated problem, which is best dealt with by numerical integration procedures. An approximate analytical solution of the problem has been published by Fannelop and Ryhming.[3]

The present article is based on Reference 4 where details may be found, in particular concerning the corresponding Fortran program 'PIPE 1'.

The major difficulty is due to the *singularity* (established in the Appendix) which results from the combined effects of friction and choking, occurring at the broken end.

0271 2091/86/020083-18$09.00

Received 8 May 1985
Revised 9 September 1985

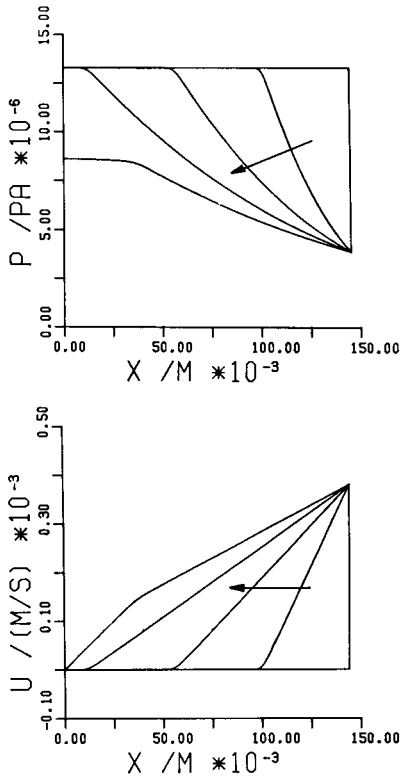

Figure 1. Homentropic flow (no friction, entropy $s(x, t) = \text{const}$). Parameter: $t = 0, 100, \ldots, 400$ s. $u_i = 0$, $4f = 0$

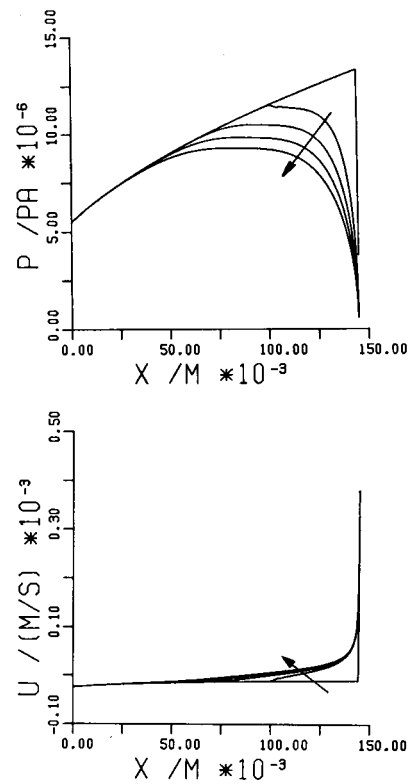

Figure 2. Flow with friction and $u < 0$ at $t = 0$. Parameter: $t = 0, 100, \ldots, 400$ s. $u_i = -10$ m/s, $4f/D = 0{\cdot}00837$/m

2. PHYSICS OF THE PROBLEM

Under normal steady-state conditions the flow will be assumed to be orientated from right ($x = L$) to left ($x = 0$) (Figures 1 and 2), i.e. in the opposite direction to the x-axis. Immediately after the rupture (assumed to occur at $x = L$), choking over the entire cross-section of the pipe* takes place there, while an expansion wave starts running from $x = L$ to the left, i.e. in the same direction as the still undisturbed stationary flow. The strong expansion produces a reversal of the flow so that there is an outflow at both ends of the pipeline.

If the flow were frictionless, the pressure distribution $p(x)$ at different times t would look as shown in Figure 1. Friction being taken into account, two facts lead to a totally different distribution (Figure 2):

(a) As a result of frictional losses the pressure gradient $(\partial p/\partial x)_t$ is positive in the flow region on the left-hand side, which the expansion wave has not yet reached.
(b) Owing to the strong expansion taking place on the right-hand side $(\partial p/\partial x)_t$ is negative.

Hence a pressure peak will appear somewhere between $x = 0$ and $x = L$. Its location $x_{p\max}$ corresponds approximately to the location of flow reversal, where the velocity is zero. With increasing time, the pressure peak will slowly move towards the left until it reaches $x = 0$. Except for these features, which have already been described in Reference 3, little seems to be known from the theoretical point of view. The main reason for this is that the problem is *highly non-linear*, making the finding of analytical solutions unlikely.†

Compared with References 3, 5, 6 (except for the last chapter) and 7, the physical model used in our study presents a basic difference: in References 3 and 5–7 the assumption of isothermal flow is made, which means that no energy equation needs to be considered. This simplifying assumption is no longer valid if important changes in the thermodynamic states of the particles occur over short distances (as in our case near the broken end of the pipeline). In the present study only the *initial conditions* (described in sections 5 and 7) are those of isothermal flow, whereas the unsteady flow generated after the rupture of the pipeline is considered as *adiabatic*.

Both assumptions (isothermal initial condition and adiabatic flow for $t > 0$) are extremely idealized, reality being somewhere in between. This heuristic choice is justified as follows:

1. Before rupture the flow is *slow* ($u \cong 10$ to 25 m/s) and the time-span $\Delta t_L (\cong 2{\cdot}5$ h) a particle takes to move along the whole pipeline is *long*. The isothermal flow distribution for the initial condition ($t = 0$s) therefore appears very plausible.
2. The sudden introduction (at $t = 0$) of the adiabatic flow hypothesis has almost no effect on the left part of the pipeline (situated between $x = 0$ and the location of the wave front). This assertion is confirmed by Figure 2 (and Figures 9–11). This feature can also be shown with a thermodynamic argument. Consider a steady, *adiabatic* pipe flow of a perfect gas with low velocities (or more correctly, low Mach numbers). If we drew the static-state line (the so-called 'Fanno-line') in Mollier's enthalpy–entropy diagram, we would see that it is almost identical to an *isothermal* line (itself identical to a constant enthalpy line).
3. It can be shown[8] that for a stationary isothermal choking condition the limiting gas velocity

* In various studies (e.g. Reference 5) mainly concerned with the *control* of unsteady flows in piping systems, their authors consider that the choked flow occurs in the open portion of a partially closed outlet valve located at $x = L$. As the Mach number on the upstream side of the valve is *low* the same authors consider an *adiabatic* acceleration through the valve. This is a totally different flow situation from ours.

† Readers with an inclination towards analytical methods should be made aware of the treatise[6] by H. Pascal, essentially devoted to unsteady gas flow in pipelines. However, the cases which are dealt with in this book are mainly restricted to quasi-steady, isothermal and low subsonic flow situations.

is $\sqrt{(RT)}$, but infinite heat transfer coefficients would be necessary. Shapiro (Reference 8, p. 183) writes that 'this limit is artificial and not physically real'. The hypothesis of adiabatic flow, especially near the broken end, where particles are accelerated relatively rapidly and (at least at the beginning) over a relatively short distance, seems closer to reality than the hypothesis of isothermal flow. For long time intervals the heat transferred into the pipeline should be accounted for, but this would considerably complicate the analysis.

It appears that laboratory tests of the class of problems investigated here cannot be performed, in view of the *enormous* length-to-diameter ratio L/D of the pipeline (order of magnitude 10^5).

3. MATHEMATICAL ASPECTS

One of the non-linear terms is the *friction term*, which appears in the suitably non-dimensionalized momentum equation as *proportional to the friction factor f and to the very high length-to-diameter ratio L/D* mentioned above.* For our application we shall use the value $fL/D \cong 300$ (see section 5).

Looking for an approximate analytical solution, Fannelop and Ryhming[3] were obliged to define three phases, each one being subjected to different simplifications and corresponding solutions: an *early-time regime* (lasting about 25 s and stretching over some 10 km, counted from the breaking point), an *intermediate-time regime* (lasting until the pressure peak reaches the low-pressure side) and a *late-time regime* (of a quasi-steady nature). Fannelop and Ryhming[3] devoted the main part of their investigation to the *late-time regime*, commenting that the other two regimes are better dealt with by numerical methods.

One advantage of the numerical approach is that is treats the *whole* time range with the *same set of equations*, in which *no term is neglected*. Furthermore, numerical methods are not limited to very simple thermodynamic models of the fluid, such as the perfect gas, but can be extended to real gases.[9,10]

4. USE OF THE METHOD OF CHARACTERISTICS

The study presented here is based on the method of characteristics.[8,11-15] This method has mainly been applied with success to fluid mechanics problems without friction, or at least with only moderate frictional effects, i.e. with relatively low values of the parameter fL/D. Cases with important frictional effects have to be carefully checked regarding the accuracy of the results (see section 9). They require many more grid points than cases without friction.

The well-established method of characteristics can be applied in various ways. Considering that the flow remains shock-free, we have chosen the 'inverse marching procedure' (also called 'mesh-type procedure' or 'method of specified time intervals'), using as basic dependent variables p, ρ and u.

To achieve high accuracy, an interpolation scheme with *second-order polynomials* had to be introduced, together with the assumption of correspondingly *curved characteristic lines* (Figure 3). For this reason the overall calculation method is comparable to a *second-order* finite difference method. More details concerning this calculation procedure can be found in Reference 16.

The case without friction (Figure 1) is well known from the theoretical point of view (see, for instance, chapter III of Reference 13). Use of the Riemann variables leads to a very simple and elegant analytical solution.

* In Reference 7 it is shown that for a certain class of unsteady low subsonic gas flow problems ('packing' and 'drafting'), fL/D is a parameter of primary importance. The calculated results presented in Reference 7 are based on the value $fL/D = 250$.

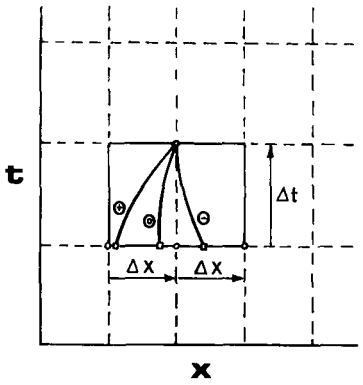

Figure 3. Elementary mesh of the wave diagram $t(x)$, showing the three *curved* characteristic lines

As already mentioned in the Introduction, the case with frictional flow (Figure 2), presents a totally different aspect, especially as far as the region near the breaking point ($x = L$) is concerned. There the pressure, density and velocity distributions (for a given time t) have *infinite values of their partial x derivatives.* (An analytical proof of this assertion is given in the Appendix.) This is a major computational difficulty. In order to cope with the latter a special procedure based on a modified flow condition for the last Δx-mesh (described in section 9) has considerably improved the accuracy and convergence of the calculation.

It should be noted that only the case where the breaking occurs on the *high-pressure* end of the pipeline has so far been investigated, as being the most significant from the safety point of view.

5. HYPOTHESIS AND BASIC NUMERICAL INPUT

The following set of data corresponds to a real case in the North Sea.

The pipeline is straight, has a length $L = 145\,\text{km}$ and a diameter $D = 0{\cdot}87\,\text{m}$.

The gas is considered as perfect, i.e. $p = \rho RT$, with $R = 518{\cdot}3\,\text{m}^2/(\text{s}^2\text{K})$ and $\kappa = c_p/c_v = 1{\cdot}33$. Starting from an isothermal initial flow distribution (discussed in section 2) with

$$T_i(x) = 281\,\text{K}, \quad (0 \leqslant x \leqslant L),$$

the flow is considered adiabatic and one-dimensional (see section 2). The remaining initial conditions (at $x = L$; see also section 7) are

$$u_i = -10\,(\text{m/s})$$
$$p_i = 133\ \text{bar}.$$

The exterior pressure will be taken as

$$p_a = 6\ \text{bar},$$

corresponding to a sea depth of $\sim 50\,\text{m}$.

The lowest Reynolds number $Re = \rho uD/\mu$, corresponding approximately to the lowest (ρu)-value, is given by the initial condition:

$$Re_i \cong \left(\frac{p_i}{RT_i}\right)\frac{u_i D}{\mu_i} \cong 7 \times 10^7.$$

For $Re > 7 \times 10^7$ the friction factor ('Fanning factor') $f = \tau_w/(\rho u^2/2)$ (where τ_w is the wall shear

stress) can be considered independent of *Re*. Making this simplifying assumption, we consider

$$f = \text{constant} = 0{\cdot}0018205,$$

which gives a pressure drop of 78 bar for the steady flow before breaking (see section 7).

This constant value of f will be used throughout the *unsteady* flow analysis.

6. CHARACTERISTIC AND COMPATIBILITY EQUATIONS

Starting from the three conservation laws (continuity, momentum and energy equations given in the Appendix), and following a classical procedure (of which a comprehensive treatment is given in Reference 15), we establish the following relations:

(a) Slopes of characteristics

$$\frac{\mathrm{d}_0 t}{\mathrm{d}_0 x} = \frac{1}{u}, \quad \frac{\mathrm{d}_+ t}{\mathrm{d}_+ x} = \frac{1}{u+a} \quad \text{and} \quad \frac{\mathrm{d}_- t}{\mathrm{d}_- x} = \frac{1}{u-a}. \tag{1), (2), (3)}$$

(The significance of $(\ldots)_0$, $(\ldots)_+$ and $(\ldots)_-$ is explained in the Nomenclature list).

(b) Compatibility equations:

$$\mathrm{d}_0 p - a^2 \mathrm{d}_0 \rho = -(\kappa - 1) u \beta \mathrm{d}_0 t, \tag{4}$$

$$\mathrm{d}_+ p + \rho a \mathrm{d}_+ u = [a - (\kappa - 1)u] \beta \mathrm{d}_+ t, \tag{5}$$

$$\mathrm{d}_- p - \rho a \mathrm{d}_- u = [-a - (\kappa - 1)u] \beta \mathrm{d}_- t, \tag{6}$$

where

$$a = \sqrt{(\kappa R T)} = \text{speed of sound}, \tag{7}$$

$$\beta = -\frac{4f}{D}\frac{\rho u |u|}{2} = \text{friction coefficient}. \tag{8}$$

The numerical resolution of this set of equations consists of replacing the differentials by finite differences and the finite quantities (such as ρ, a, u, β) by well-defined 'average values'.

The emphasis of this article is on describing the *physics* of the problem and the *results* obtained. For more details on the computational aspects of the solution procedure the reader is referred to Reference 4.

7. INITIAL CONDITIONS

For $0 \leqslant x \leqslant L$ (Figure 4) we shall assume a *steady isothermal flow* from right to left. The combination of the continuity and momentum equations (see section 6.4 of Reference 8 for example) gives (neglecting the term $\ln(Ma/Ma_i)^2$)

$$\left[\frac{Ma}{Ma_i}\right]_{t=0} = \left[\frac{u}{u_i}\right]_{t=0} = \left[\frac{p}{p_i}\right]_{t=0}^{-1} = \left[1 - \kappa Ma_i^2 \frac{4f}{D}(L - x)\right]_{t=0}^{-1/2}. \tag{9}$$

Introducing the data from section 5 we obtain $p_{\substack{x=0 \\ t=0}} = 55$ bar (point ⓓ of Figure 4).

In our simplified physical model the sudden rupture at the high-pressure end occurring at $t = 0$s will be accompanied by an instantaneous drop in static pressure from $p_i = 133$ bar to a much lower pressure $p_{\substack{x=L \\ t=0}}$ (point ⓑ of Figure 4) corresponding to choked flow ($Ma_{x=L} = 1$ for $t > 0$s).

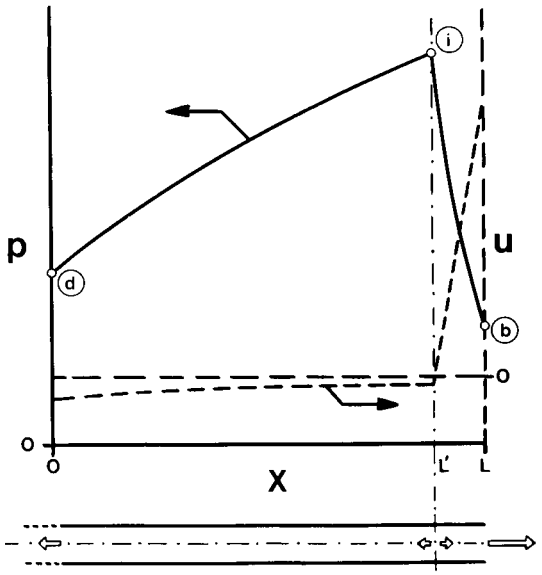

Figure 4. Initial state $p(x)$ and $u(x)$: $T(x) = \text{constant} = T_i$

The initial values $p_{t=0}(x)$, $\rho_{t=0}(x)$, $a_{t=0}(x)$ and $u_{t=0}(x)$ for $L' \leqslant x \leqslant L$, (whereby the arbitrary value $L - L'$ may cover one or more Δx-meshes) will be evaluated as follows: we assume that between L and L' (Figure 4) we have a homogeneous frictionless flow field with a velocity $u_i (= -10\,\text{m/s}$, see section 5). Let $\Delta t^* (> 0)$ be the time an expansion wave would take to travel from $x = L$ to $x = L'$. If such an expansion wave starts from $x = L$ at $t = -\Delta t^*$, we obtain a homentropic expansion flow, with a pressure and velocity distribution at $t = 0$ as shown in Figure 4 (points ⓑ to ⓘ). Such flows are well known from the theoretical point of view.[13,14] Their analysis, best conducted using the 'Riemann variables', leads to the following relations:

$$u_{t=0} = \frac{2}{\kappa+1}\left(1 + \frac{\kappa-1}{2}\frac{u_i}{a_i} - \frac{1-\xi}{\tau_i}\right)a_i, \tag{10}$$

$$a_{t=0} = \left[1 - \frac{\kappa-1}{2}\left(\frac{u_{t=0} - u_i}{a_i}\right)\right]a_i, \tag{11}$$

$$\rho_{t=0} = \left[\frac{a_{t=0}}{a_i}\right]^{2/(\kappa-1)}\left(\frac{p_i}{RT_i}\right), \tag{12}$$

$$p_{t=0} = \left[\frac{a_{t=0}}{a_i}\right]^{2\kappa/(\kappa-1)} p_i, \tag{13}$$

where

$$a_i = \sqrt{(\kappa R T_i)}, \quad \tau_i = \frac{\Delta t^*}{L/a_i} \quad \text{and} \quad \xi = \frac{x}{L}.$$

These relations actually describe a self-similar motion, the similarity parameter being $(1 - \xi)/\tau_i$ (see p. 192 of Reference 13).

Returning to the physical situation of the assumed sudden break at $x = L$, it appears that friction would play only a very minor role during the first few seconds. The above homentropic flow model

should therefore be a fairly good description of the starting process. The initial values for $L' \leqslant x \leqslant L$ stated above will therefore be determined with the relations (10) to (13).

The arbitrary choice of the initial flow distribution for $L' \leqslant x \leqslant L$ actually has only a slight influence on the later calculation (say for $t > 5$ s), because we have an *outflow*. The flow particles initially located between L' and L are swept out of the pipeline after a very short time interval.

8. BOUNDARY CONDITIONS

For the subsonic outflow at the low-pressure end ($x = 0$) two basic options have been implemented:

(a) prescription of the static pressure as a function of time
(b) prescription of the velocity, which is reduced to zero in an arbitrary time span, thus simulating the closing of a valve.

At the high-pressure end ($x = L$) two distinct time sequences are considered. As long as the pressure $p_{x=L}$ is higher than the external pressure in the water ($p_a = 6$ bar), there will be choking of the flow, characterized by

$$Ma_{x=L}(t) = 1. \tag{14}$$

We call this the '1st time sequence'. The condition (14) together with the compatibility equations (4) and (5) for the 0 and + characteristics form a non-linear set of three equations leading (after elimination of the unknowns p and ρ) to a 3rd-order equation with the velocity u as the remaining unknown.

The numerical results show that during the 1st time sequence described above, the pressure and density at $x = L$ decrease (relatively slowly) with time. This is directly connected with the fact that the flow presents *friction*. (In the case of a homentropic, i.e. frictionless, flow $p_{x=L}(t)$, $\rho_{x=L}(t)$ and $u_{x=L}(t)$ would remain constant.)

When $p_{x=L}(t)$ reaches the exterior pressure p_a (input value; see section 5), the choking condition no longer holds and is (automatically) replaced by the classical 'equal pressure' condition:

$$p_{x=L}(t) = p_a (= \text{constant}). \tag{15}$$

This condition characterizes our '2nd time sequence'. It leads to a *subsonic outflow*, similar to that already described under (a) (the velocity is of course orientated in the other direction).

9. ACCURACY, CONVERGENCE AND STABILITY

Checking the accuracy of a computed solution has basically two aspects: (a) the solution can be compared with experimental results, if such results are available; (b) various computational checks can be investigated. For the reasons explained at the end of section 2, no type (a) control could be done.

A convenient and severe type (b) check is provided by the evaluation of an 'accuracy criterion' ε, which is now described. Its physical interpretation based on the law of 'conservation of mass' is basically the same as the one used in Reference 3: let M be the mass of gas contained in the entire pipeline at the time t. At some later time $t + \Delta t$, the mass in the pipeline will be M'. The loss of mass in the pipeline from t to $t + \Delta t$ is therefore $M - M'$ (> 0) (Figure 5).

It must be equal to the integrated mass flow having left the pipeline at both ends during Δt:

$$\Delta M = -\int_{\tau=t}^{t+\Delta t} \dot{M}_{x=0} \mathrm{d}\tau + \int_{\tau=t}^{t+\Delta t} \dot{M}_{x=L} \mathrm{d}\tau,$$

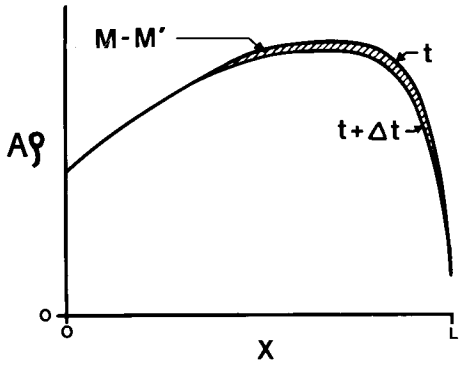

Figure 5. Graphical interpretation of $M - M'$

where $\dot{M} = A\rho u$ and τ = time (integration variable)

The 'accuracy criterion' is defined as

$$\varepsilon = \frac{M - M'}{\Delta M} \quad \text{(ideal value = 1)}, \tag{16}$$

with ΔM and Δt corresponding to *one* time step in the calculation. We consider that the *overall* calculation 'converges' if, as N (the number of grid points) increases, ε tends towards 1.

The author would like to suggest a systematic use of this ε for all unsteady one-dimensional flow calculations where this quantity makes sense.

The basic numerical case defined in section 5, and calculated with $N = 401$, has given ε-values of less than 1·02, which corresponds to a relative 'error' $(\varepsilon - 1)$ of 2 per cent.

Next we describe the 'modified flow condition' for the last Δx-mesh (or 'reach') mentioned in section 4. If we multiply by the empirical 'convergence acceleration factor' K_f the friction terms of the compatibility equations (4) and (5), which, together with (14), govern the flow calculation of the last mesh, we obtain the results shown in Figure 6.

The value $K_f = 1$ leaves the relations unchanged, whereas the value $K_f = 0$ indicates that the viscous terms are completely omitted.

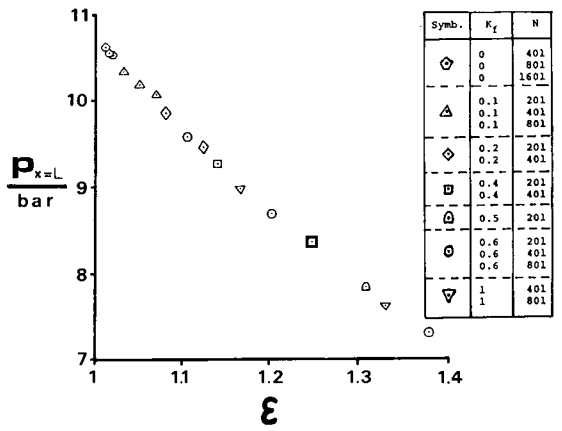

Figure 6. Convergence test for K_f. Time $t = 100$ s and time-step $\Delta t = 100$ s/$(N - 1)$. Choked flow at $x = L$

The idea behind the introduction of this K_f is based on the following considerations:

(a) As $N \to \infty$, the last mesh becomes so small that the influence *on the overall result*, due to the K_f-value used, should vanish.
(b) Even though $|(\partial p/\partial x)_{x=L}|$ may be quite large for a non-viscous flow, it is not infinite (see Figure 1).
(c) From the numerical point of view very large numbers may be handled, infinite ones not.

Figure 6 also shows the influence of the number of grid points N on the convergence. If N increases (K_f remaining constant), or if K_f approaches 0 (N remaining constant), the value of the accuracy criterion ε tends towards its ideal value $\varepsilon_{ideal} = 1$, whereas $p_{x=L}$ seems to approach a limiting value. The value $K_f = 0$ was therefore selected for the calculations in sections 10 and 11.

In order to ensure *numerical stability* the classical Courant–Friedrichs–Lewy (CFL) stability criterion,[17,18] prescribing a maximum value for the time step Δt, has been used:

$$\Delta t \leqslant \Delta t_{CFL} = \frac{\Delta x}{(|u| + a)_{max}}, \tag{17}$$

where Δx is the mesh size along the axis of the pipeline. The same basic numerical case (mentioned above) was run with $\Delta t = 0{\cdot}25$ s, considering that Δt_{CFL} was evaluated at 0·48 s.

10. TEST CASES

Case 1. *Frictionless flow* ($4f/D = 0$) *with gas initially at rest* ($u_i = 0$)

This case is represented in Figure 1. Except for the slight rounding-off of the curves at the wave front, the computational result corresponds very well to the analytical solution, equations (10)–(13). In particular, for the case considered (where $N = 401$), the propagation speed of the wave front is equal, within an error of 1 per cent, to the theoretical value $a_i = \sqrt{(\kappa R T_i)}$.

This control is also satisfied in cases with friction ($(4f/D) \neq 0$) and $u_i = 0$.

The frictionless flow case corresponds to the simple wave solution. For this classical case,[8,11–15] the 'characteristic lines' in the wave diagram $t(x)$ are straight and correspond to constant pressure lines. This is yet another check on the numerical procedure, the result of which was completely satisfactory.

Case 2. *Detailed representation of the 'kink'*

All cases with friction show an unexpected flow distribution near the front of the expansion wave. In particular the $p(x)$ curves present a sort of 'kink'. Calculations with very high accuracy (because of a very high value of N/L) indicate that this feature is not due to a numerical effect, but corresponds to a real physical situation. A closer inspection of the corresponding flow section shows that the middle of the kink corresponds approximately to the location of *flow reversal* ($u = 0$, $(\partial u/\partial x)_t > 0$). In this region the frictional term is very small and the flow is nearly isentropic, but not homentropic. For a homentropic flow the relations (10)–(13) give roughly twice as steep values of $(\partial p/\partial x)_t$ at the wave front.

Figure 7 shows the *formation* of the kink during the first 45 seconds after the break. As time passes the amplitude of the kink is reduced, due to frictional effects (see also Figure 2).

According to Reference 19 this special behaviour is due to the fact that the problem is *singular* in nature and can be dealt with analytically by using the 'method of matched asymptotic expansions'.

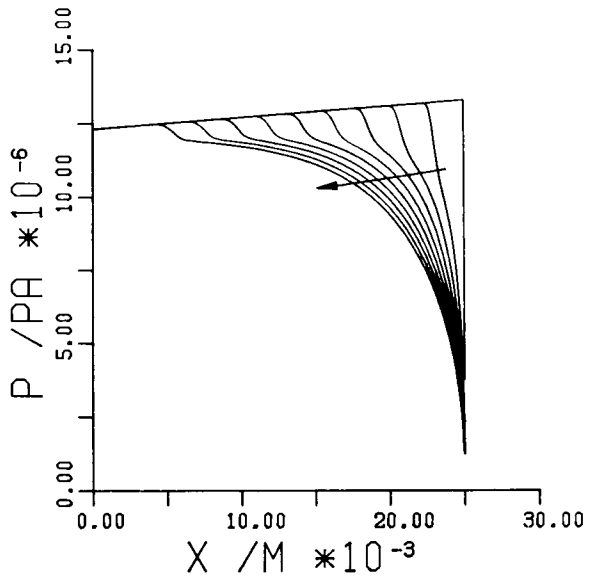

Figure 7. Formation of the 'kink'. Parameter: $t = 0{\cdot}5, \ldots, 45$ s. $u_i = -10$ m/s, $4f/D = 0{\cdot}00837$/m

This mathematical method (a full description of which can be found in Reference 20) uses so-called inner and outer expansions, which need to be matched in the overlap domain.

Some more descriptive details of this kink are given in section 11—Case 4.

11. DISCUSSION OF REALISTIC CASES

Case 3. Shutting the valve at the low-pressure side

As is well known from hydraulics,[21] such a manoeuvre would be followed by a pressure build-up upstream of the valve. Case 3 corresponds to the basic case of section 5, except for the valve being shut abruptly at $t = 0$, and we find (Figure 8) $[p_{x=0}(t)]_{\max} \cong 90$ bar at $t \cong 600$ s.

The $p(x)$ distribution for the higher time values is typical for what has been termed 'late-time regime' and investigated analytically in Reference 3.

Case 4. Practical case corresponding to North Sea conditions

The numerical input has been described in section 5. Figure 2 gives the pressure and velocity distributions. The former shows a point of maximum pressure which slowly moves towards the low-pressure side, as already mentioned in section 2. The point of flow reversal is nearby, though not at exactly the same location. The left-hand side of the 'kink' referred to in section 10 represents the front of the expansion wave. It is interesting to note that even in the presence of friction it travels (from right to left) at the speed of sound with respect to the gas, which itself moves in the same direction (see also the corresponding comment in section 10—Case 1). As the kink (which at first has a negative $\partial p/\partial x$ value) moves faster than the pressure peak, the latter is left behind. While the distance separating the kink from the pressure peak increases, the kink tilts down to the other side: its $\partial p/\partial x$ is now positive. During this latter phase its amplitude seems to be gradually smoothed by frictional effects.

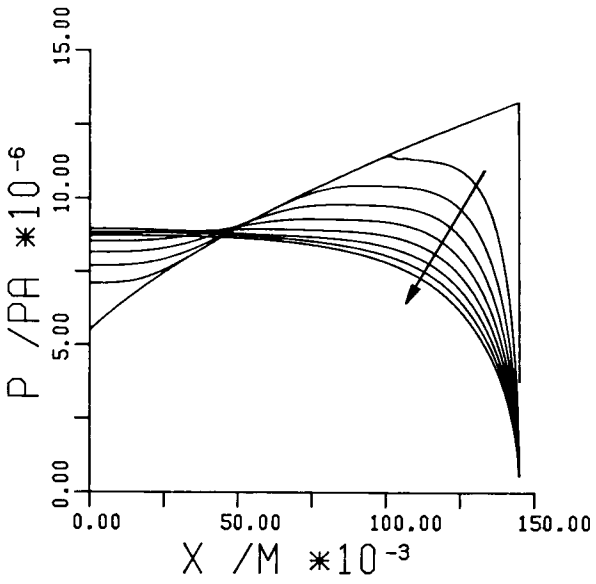

Figure 8. Pressure distribution after shutting the valve at $x = 0$ and $t = 0$. Parameter: $t = 0, 100, \ldots, 800$ s. $u_i = -10$ m/s, $4f/D = 0{\cdot}00837$/m

Figure 9 shows the stream density distribution

$$\rho u = \frac{\dot{M}}{A} = f(x, t).$$

The *critical speed of sound* distribution of Figure 10 also gives (indirectly) the *stagnation temperature* distribution, as

$$a^* = \sqrt{\left(\frac{2\kappa}{\kappa + 1} RT_u\right)}. \tag{18}$$

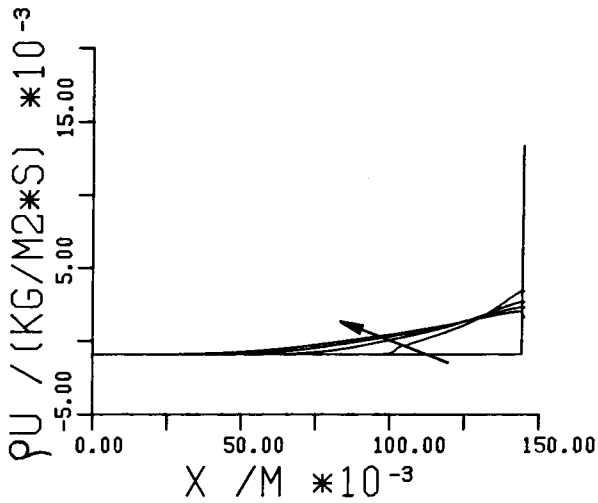

Figure 9. Stream density (ρu) distribution of case 4. Parameter: $t = 0, 100, \ldots, 400$ s. $u_i = -10$ m/s, $4f/D = 0{\cdot}00837$/m

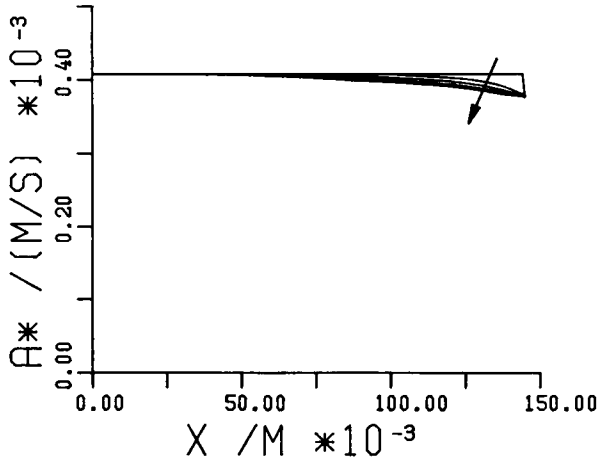

Figure 10. Critical speed of sound (a^*) distribution of case 4. Parameter: $t = 0, 100, \ldots, 400$ s. $u_i = -10$ m/s, $4f/D = 0{\cdot}00837$/m

All values of a^* (and T_u) lie in a narrow band:

$$T_{u,\max}/T_{u,\min} \cong T_i/T_{u,x=L} \cong 1{\cdot}16.$$

The *stagnation pressure* distribution,

$$p_u = \left[1 + \frac{\kappa - 1}{2} Ma^2\right]^{\kappa/(\kappa-1)} p = f(x, t), \tag{19}$$

looks very similar to the static pressure distribution. However, although $(\partial p/\partial x)_{x=L} = -\infty$, it can be shown analytically that for choking $(\partial p_u/\partial x)_{x=L}$ has a finite value.

Figure 11 gives the *non-dimensionalized entropy variation*, defined as

$$\frac{s - s_i}{R} = \ln\left[\left(\frac{T}{T_i}\right)^{\kappa/(\kappa-1)} \Big/ \left(\frac{p}{p_i}\right)\right]. \tag{20}$$

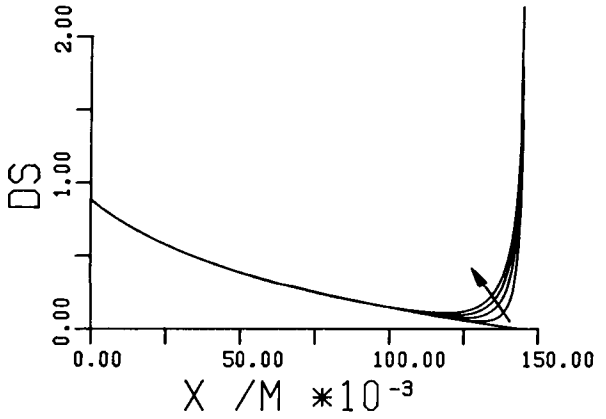

Figure 11. Non-dimensionalized entropy ($s - s_i/R$) distribution of case 4. Parameter: $t = 0, 100, \ldots, 400$ s. $u_i = -10$ m/s, $4f/D = 0{\cdot}00837$/m

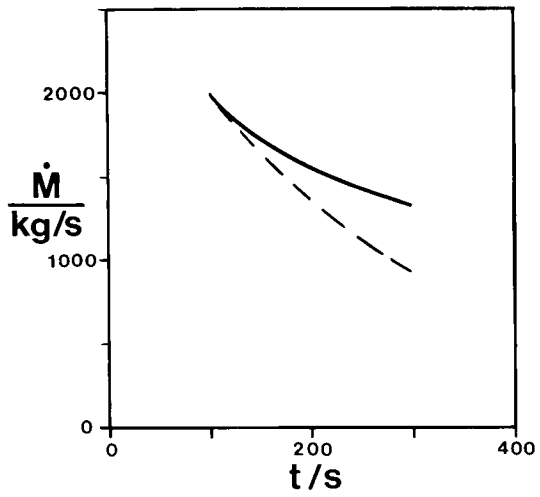

Figure 12. Mass-flow rate at $x = L$ as a function of time

As pointed out in the Introduction, knowledge of the *mass-flow rate $\dot{M}$ at the break point, as a function of time*, is of great practical interest to the offshore gas industry. The continuous line in Figure 12 shows this relationship for $t = 100$ to 300 s. The broken line in Figure 12 represents a pure exponential passing through the point $\dot{M}(t = 100\,\text{s})$ and having the same derivative at this point. The comparison of the two curves shows that the decay of $\dot{M}(t)$ is 'slower' than exponential.

It is not the purpose of this article to discuss the security measures which ought to be taken to prevent the hazards (mentioned in the Introduction) to which oil-rigs or ships might be exposed.

12. CONCLUSIONS

(a) In order to evaluate the safety and pollution problems due to the rupture of an offshore gas pipeline it is necessary to understand the unsteady fluid dynamics behaviour occurring inside the pipeline. The associated mathematical formulation is highly non-linear and no analytical solution for it is yet known. Nor can laboratory tests be used. The best approach therefore is one based on computational fluid dynamics.

(b) This article describes results obtained with a Fortran program (PIPE 1), based on the method of characteristics, with which the distribution of thermodynamic quantities such as $p(x, t)$, $u(x, t)$, etc. can be calculated. The algorithms used are however limited to shock-free flows.

(c) An accuracy criterion shows that high numerical accuracy may be obtained if the number of grid points is sufficiently large and if a special modified form of the boundary condition at the broken section is used.

(d) The results confirm conclusions already established by Fannelop and Ryhming[3] that frictional flows with large values of $4fL/D$ (order of magnitude: 1000) behave very differently from flows without friction. In particular, the mass flow escaping through the broken section and the pressure there fall to much smaller values.

(e) On the other hand, at some distance from the broken section (compare for example Figures 2 and 1 at $x = 0{\cdot}9\text{L}$), the pressure stays at high values much longer than in the case without friction.

(f) As computing time is considerable for long pipelines and long physical times, it may be advantageous to use the PIPE 1 program only for the time phases preceding the 'late time regime', and evaluate the latter with the analytical solution developed in Reference 3.
(g) The weakest aspect of the physical model used is the perfect gas assumption (section 5). Therefore, a real gas version of the computer program has been developed (PIPE 2).[9,10] One of its results is that the mass flow of methane escaping from the pipeline is about 25 per cent larger than that obtained with PIPE 1.

ACKNOWLEDGEMENTS

This research is complementary to the study described in Reference 3. The basic structure was defined by Prof. I. L. Ryhming, IMHEF (Institut de Machines, Hydrauliques et de Mécanique des Fluides), Swiss Federal Institute of Technology of Lausanne. The author would like to acknowledge the valuable advice given to him by Prof. Ryhming throughout the course of this study.

NOMENCLATURE

A	cross-section
a	speed of sound, equation (7)
a^*	critical speed of sound, equation (18)
D	diameter of pipeline
f	friction factor (Fanning factor), section 5
K_f	convergence acceleration factor, section 9
L	length of pipeline
M	mass inside pipeline, section 9
$\dot{M}$	$= A\rho u$, mass-flow
Ma	Mach number
N	number of grid points
$p; p_a$	pressure; exterior pressure
R	$= p/(\rho T)$ gas constant
s	entropy/mass
T	absolute temperature
t	time
u	velocity of gas
x	axis along pipeline (orientated from the low-pressure end towards the high-pressure end)
β	friction coefficient, equation (8)
ε	accuracy criterion, equation (16)
κ	$= c_p/c_v$, ratio of specific heats
μ	dynamic viscosity
ρ	density
τ_w	tangential stress at the wall

Subscripts

$(\ldots)_i$	initial value, sections 5 and 7
$(\ldots)_t$	$(\partial\ldots/\partial t)_x$ partial derivative
$(\ldots)_u$	total (or stagnation) state

$(\ldots)_x$	$(\partial\ldots/\partial x)_t$ partial derivative
$d_0(\ldots)$	differential along pathline 0
$d_+(\ldots)$	differential along + characteristic
$d_-(\ldots)$	differential along − characteristic

APPENDIX—PROOF OF THE SINGULARITY AT $Ma = 1$

For an adiabatic flow of a perfect gas through a constant area pipe the conservation laws can be formulated as follows: (see, for instance Reference 15, chapter 19).

Continuity equation

$$\rho_t + u\rho_x + \rho u_x = 0.$$

Momentum equation

$$\rho u_t + \rho u u_x + p_x = -\frac{\rho u^2}{2}\frac{4f}{D}.$$

Energy equation

$$(p_t + up_x) - a^2(\rho_t + u\rho_x) = (\kappa - 1)\frac{\rho u^3}{2}\frac{4f}{D}.$$

Dividing these relations by ρu, $\rho u^2 (= \kappa p Ma^2)$ and $\rho u a^2 (= \kappa u p)$, respectively, we obtain after minor rearrangements

$$\left.\begin{aligned} \frac{\rho_x}{\rho} + \frac{u_x}{u} &= K_1 \text{ with } K_1 = -\frac{1}{u}\frac{\rho_t}{\rho}, \\ \frac{1}{\kappa Ma^2}\frac{p_x}{p} + \frac{u_x}{u} + \frac{1}{2}\frac{4f}{D} &= K_2 \text{ with } K_2 = -\frac{1}{u}\frac{u_t}{u}, \\ \frac{1}{\kappa}\frac{p_x}{p} - \frac{\rho_x}{\rho} - \frac{\kappa - 1}{2}Ma^2\frac{4f}{D} &= K_3 \text{ with } K_3 = -\frac{1}{\kappa u}\frac{p_t}{p} + \frac{1}{u}\frac{\rho_t}{\rho}. \end{aligned}\right\} \tag{21}$$

From the equation of state $\rho = p/(RT)$ we obtain

$$\frac{\rho_x}{\rho} = \frac{p_x}{p} - \frac{T_x}{T} \tag{22}$$

and from $u = aMa = \sqrt{(\kappa RT)}\, Ma$ we obtain

$$\frac{u_x}{u} = \frac{1}{2}\frac{T_x}{T} + \frac{Ma_x}{Ma}. \tag{23}$$

Elimination of ρ_x/ρ and u_x/u between (21)–(23) and setting $p_x/p = \pi$, $T_x/T = \tau$ and $Ma_x/Ma = \mu$, (21) becomes

$$\left.\begin{aligned} \pi - \tfrac{1}{2}\tau + \mu &= K_1, \\ \frac{1}{\kappa Ma^2}\pi + \tfrac{1}{2}\tau + \mu &= -\frac{1}{2}\frac{4f}{D} + K_2, \\ -\frac{\kappa - 1}{\kappa}\pi + \tau &= \frac{\kappa - 1}{2}Ma^2\frac{4f}{D} + K_3. \end{aligned}\right\} \tag{24}$$

This linear system of equations can be solved for the three unknowns π, τ and μ. The results, written in terms of p_x, T_x, Ma_x and u_x are

$$\frac{\partial p}{\partial x} = p\left[-\frac{\kappa Ma^2[1-(\kappa-1)Ma^2]}{2(1-Ma^2)}\frac{4f}{D} - \frac{\kappa Ma^2}{1-Ma^2}(K_1 - K_2 + K_3)\right], \tag{25}$$

$$\frac{\partial T}{\partial x} = T\left[-\frac{\kappa(\kappa-1)Ma^4}{2(1-Ma^2)}\frac{4f}{D} - \frac{\kappa Ma^2 - 1}{1-Ma^2}(K_1 - K_2 + K_3) - (K_1 - K_2)\right], \tag{26}$$

$$\frac{\partial(Ma)}{\partial x} = Ma\left[\frac{\kappa Ma^2\left(1+\frac{\kappa-1}{2}Ma^2\right)}{2(1-Ma^2)}\frac{4f}{D} + \frac{1+\frac{\kappa-1}{2}Ma^2}{1-Ma^2}K_1 - \frac{(\kappa+1)Ma^2}{2(1-Ma^2)}K_2 + \frac{1+\kappa Ma^2}{2(1-Ma^2)}K_3\right], \tag{27}$$

$$\frac{\partial u}{\partial x} = u\left[\frac{\kappa Ma^2}{2(1-Ma^2)}\frac{4f}{D} + \frac{1}{1-Ma^2}(K_1 - K_2 + K_3) + K_2\right]. \tag{28}$$

It is evident that all these partial derivatives tend towards infinity, as Ma tends towards 1, provided that $4f/D \neq 0$. This establishes the expected singularity.

Remarks

1. Some special cases of *unsteady* flows with $4f/D = 0$ (homentropic flows with uniform initial conditions) would lead to $K_1 = K_2 = K_3 = 0$. For these cases the above relations (25)–(28) would be *indefinite* ($(\partial\ldots/\partial x) = (0/0)$) at $Ma = 1$. An analysis similar to the one which led to the equations (10)–(13) would show that, for $Ma = 1$, $(\partial\ldots/\partial x) = f(\kappa)$ has a finite value.
2. In the case of *steady flows* $K_1 = K_2 = K_3 \equiv 0$ and the equations (25)–(28) degenerate to particular cases of the well-known relations given in textbooks, such as References 8 and 15, under the heading 'generalized one-dimensional flows'. The multiplying factors of $4f/D$ are usually called 'influence coefficients'.
3. Equation (28) shows that the often encountered simplifying assumption

$$\frac{Du}{Dt} = \frac{\partial u}{\partial t} + u\frac{\partial u}{\partial x} \cong \frac{\partial u}{\partial t}$$

(see for instance Reference 21, chapter 15, p. 273) is valid only for $Ma \ll 1$. It would be totally incorrect at $Ma \gtrsim 1$!

REFERENCES

1. O. Mundheim, *et al.*, 'Offshore blowout control', Otter Group, *Report No. STF 88 A81004*, Trondheim, Norway, 1981.
2. R. Flatt, 'Comments on a device for controlling blowouts of oil and/or gas', *Europipe '83 Conference*, 20–22 June 1983, Basle, Switzerland, Access Conference Ltd., Bucks, England, 1983, paper No. 4, pp. 23/30.
3. T. K. Fannelop and I. L. Ryhming, 'Massive release of gas from long pipelines', *Journal of Energy*, **6**, (2), 132–140 (1982).
4. R. Flatt, 'Numerical study of the unsteady flow of a perfect gas in a pipeline', *Internal Report No. A-82-6*, LMF-EPFL, Lausanne, September 1982.
5. M. A. Stoner, 'Analysis and control of unsteady flows in natural gas piping systems', *Ph.D. Thesis*, University of Michigan, Civil Eng. Dept., 1968.
6. H. Pascal, *Ecoulement non permanent dans les gazoducs*, Editions Technip, Paris, translated from Rumanian, 1972.
7. N. De Nevers and A. Day 'Packing and drafting in natural gas pipelines', *J. Petroleum Technology*, (March) 655–658 (1983).
8. A. H. Shapiro, *The Dynamics and Thermodynamics of Compressible Fluid Flow*, Vol. I, Ronald Press, 1953.

9. R. Flatt, 'Numerical study of the unsteady flow of a real gas (methane CH_4) in a pipeline', *Internal Report No.* T-83-2, *LMF-EPFL*, Lausanne, Feb. 1983.
10. R. Flatt, 'Zur Anwendung numerischer Verfahren der Strömungslehre in der Realgasdynamik' (on the application of numerical methods to the dynamics of real gases'), *Forsch. Ing.-Wes.*, **51,** (2), (1985).
11. E. Becker, *Gasdynamik*, Teubner-Verlag, 1965.
12. R. Courant and K. O. Friedrichs, *Supersonic Flow and Shock Waves*, Vol. 1 of the series 'Pure and applied mathematics', edited by H. Bohr, R. Courant and J. J. Stokker, Interscience Publishers Inc., New York, 1948. Re-edited as Vol. 21 of the series 'Applied mathematical sciences', Springer-Verlag, 1974.
13. K. Oswatitsch, *Grundlagen der Gasdynamik*, Springer-Verlag, 1976.
14. G. Rudinger, *Nonsteady Duct Flow: Wave Diagram Analysis*, Dover Publ. Inc., 1969.
15. M. J. Zucrow and J. D. Hoffman, *Gas Dynamics*, Vols. 1 and 2, J. Wiley, 1976.
16. R. Flatt, 'A singly-iterative second order method of characteristics for unsteady compressible one-dimensional flows', to be published in *Communications in Applied Numerical Methods*, **1,** 269–274 (1985).
17. R. Courant, K. O. Friedrichs and H. Lewy, 'Ueber die partiellen Differenzialgleichungen der mathematischen Physik', *Mathematische Annalen*, **100,** 32–74 (1928).
18. R. D. Richtmyer and K. W. Morton, *Difference Methods for Initial-value Problems*, 2nd edition, Interscience Publishers, 1967.
19. I. L. Ryhming, Personal communication, Fluid Mechanics Lab., Swiss Federal Institute of Technology of Lausanne, June 1983.
20. M. Van Dyke, *Perturbation Methods in Fluid Mechanics*, The Parabolic Press, Stanford, California, 1975.
21. E. B. Wylie and V. L. Streeter, *Fluid Transients*, McGraw-Hill, 1978.